

Sources of spatial variability in light absorbing components along an equatorial transect from 165°E to 150°W

Jennifer Simeon¹ and Collin Roesler²

Department of Marine Sciences, University of Connecticut, Groton, Connecticut, USA

W. Scott Pegau³

College of Oceanic and Atmospheric Sciences, Oregon State University, Corvallis, Oregon, USA

Cécile Dupouy

Centre IRD de Noumea, Noumea, New Caledonia

Received 27 August 2002; revised 28 April 2003; accepted 30 June 2003; published 25 October 2003.

[1] Spatial variability of major light-absorbing components in seawater was analyzed at the equator from 165°E to 150°W during the Zonal Flux Cruise aboard the R/V Thompson from 20 April to 10 May 1996. Spectral absorption coefficients were separated into phytoplankton, nonphytoplankton chromophoric particulate material (CPM) and chromophoric dissolved organic material (CDOM). CPM and phytoplankton absorption account for about 20% and 80% of the total particulate absorption, respectively, above 100 m. The <0.2 μm CDOM absorption accounts for nearly 80% of the total absorption below 100 m. A significant portion of spatial variability in particulate absorption was due to conservative processes in the upper 100 m. Non-conservative spatial variability of phytoplankton absorption was zonally determined by the biomass changes of a spectrally invariant taxonomic community and vertically by photoacclimation. Distributions of size-fractionated CDOM absorption are suggestive of the presence of new (0.2 to 0.7 μm) and old (<0.2 μm) DOM pools. Photochemical reactions and microbial activity are nonconservative processes that act upon these pools, respectively. New DOM was found primarily in the upper water column, while an analysis of variance showed that <0.2 μm CDOM originating from deep water composes the background CDOM in the Equatorial Pacific. *INDEX TERMS*: 4231 Oceanography: General: Equatorial oceanography; 4552 Oceanography: Physical: Ocean optics; *KEYWORDS*: Ocean optical properties, equatorial Pacific, water mass analysis, ocean tracers

Citation: Simeon, J., C. Roesler, W. S. Pegau, and C. Dupouy, Sources of spatial variability in light absorbing components along an equatorial transect from 165°E to 150°W, *J. Geophys. Res.*, 108(C10), 3333, doi:10.1029/2002JC001613, 2003.

1. Introduction

[2] Refining our understanding of the optically clear open ocean is necessary for a solid foundation of further studies in coastal ocean optics. The equatorial Pacific is an area where local physical [Wyrki and Kilonsky, 1984], biological [Landry *et al.*, 1997], chemical [Murray *et al.*, 1994] and geologic processes [Honjo *et al.*, 1982] have been well documented. Recent investigations of the bio-optical processes indicate that such studies can contribute to understanding the distribution and fluxes of biogeochemically important compounds in the equatorial Pacific (see review

in Bricaud *et al.* [2002]). In this study we investigate the distribution and spatial variability in the major light absorbing components with the goal to ascribe this variability to the underlying biological, chemical and/or physical processes characteristic of the equatorial system. The outcome from these investigations can contribute to our understanding of remotely sensed optical signatures as well as provide input parameters for bio-optical models of primary productivity and carbon cycling in the open ocean.

[3] The equatorial Pacific is a region that can drastically influence the global climate. The complex system of currents in the equatorial Pacific interacts with the atmosphere to produce climatological effects on a variety of timescales. The major currents at the equator are the South Equatorial Current (SEC), Equatorial Undercurrent (EUC), and Equatorial Intermediate Current (EIC). The SEC is a westward surface current, with northern (SEC1) and southern (SEC2) branches. The SEC2 is associated with the upwelling or “cold tongue”. The EUC flows rapidly eastward at a depth of 120 m, generating a high shear zone at the base of the

¹Now at Atmospheric and Oceanic Sciences Program, Princeton University, Princeton, New Jersey, USA.

²Now at Bigelow Laboratory for Ocean Sciences, West Boothbay Harbor, Maine, USA.

³Now at Kachemak Bay Research Reserve, Homer, Alaska, USA.

surface currents [Reverdin *et al.*, 1994]. The EIC is located beneath the EUC. The reader is referred to Wyrski and Kilonsky [1984] for further details.

[4] Light absorption, scattering and attenuation processes are measured as inherent optical properties (IOPs) of a water body, dependent upon the molecular structure of water and the associated particulate and dissolved substances. Changes in the magnitude of the absorption coefficient result generally from cumulative changes in the concentration of absorbing materials, while variations in the spectral shape become the unique signatures of chromophoric materials [Carder *et al.*, 1989; Roesler *et al.*, 1989; Babin and Stramski, 2002; Babin *et al.*, 2003]. Major light-absorbing components are categorized as water, phytoplankton, non-algal chromophoric particulate matter (CPM), and chromophoric dissolved organic matter (CDOM). The dominant light absorbing components in the open ocean are phytoplankton and their derivative CPM and CDOM products [Morel and Prieur, 1977].

[5] Many diverse processes influence the distributions of chromophoric components in the open ocean. Spatial variations in IOPs can be caused by both conservative and nonconservative changes in the proportions of the major light-absorbing components [Roesler *et al.*, 1997; Sosik *et al.*, 2001]. IOPs are categorized as passive tracers, which do not act upon the physical dynamics, but are subject to it. Redistribution of a passive tracer by diffusion, mixing and/or advection is considered a conservative change in the local concentration of the passive tracer. In theory, if the process is truly conservative, the physical mixing of one or more water types will result in the linear superposition of the end-member tracer properties. Non-conservative variability is generally associated with biological or chemical processes that effect compositional changes in the passive tracer. Some examples include preferential production or removal of CPM [e.g., Siegel *et al.*, 1989; Stramski *et al.*, 1992], photo-bleaching of CDOM [Mopper *et al.*, 1991; Miller and Moran, 1997], local phytoplankton growth, phytoplankton photoacclimation, or changes in the species composition in the phytoplankton community [e.g., Stramski and Reynolds, 1993, 1995, 2001].

[6] The goals of this study are to (1) quantify the relative contributions of CDOM, CPM and phytoplankton to absorption, (2) identify conservative behavior of each major component with respect to the hydrography within the transect, (3) identify the sources of nonconservative behavior in the absorbing components within the upper 250 m of the equatorial Pacific, from 165°E to 150°W.

2. Methods

[7] From 20 April to 10 May 1996, ten stations spaced $\sim 5^\circ$ apart, were sampled along the equator from 165°E to 150°W during the Zonal Flux cruise (TN060) on the R/V Thompson (Figure 1). Analysis for this study was restricted to hydrocasts and optical casts occurring between the hours of 1000 to 1200, local time, to reduce diurnal effects and to minimize the time between the in situ optical observations and the discrete-sample optical measurements from the hydrocasts.

2.1. Discrete Water Measurements

[8] Seawater samples were collected in 30-L Go Flo bottles seated on a rosette equipped with a CTD and

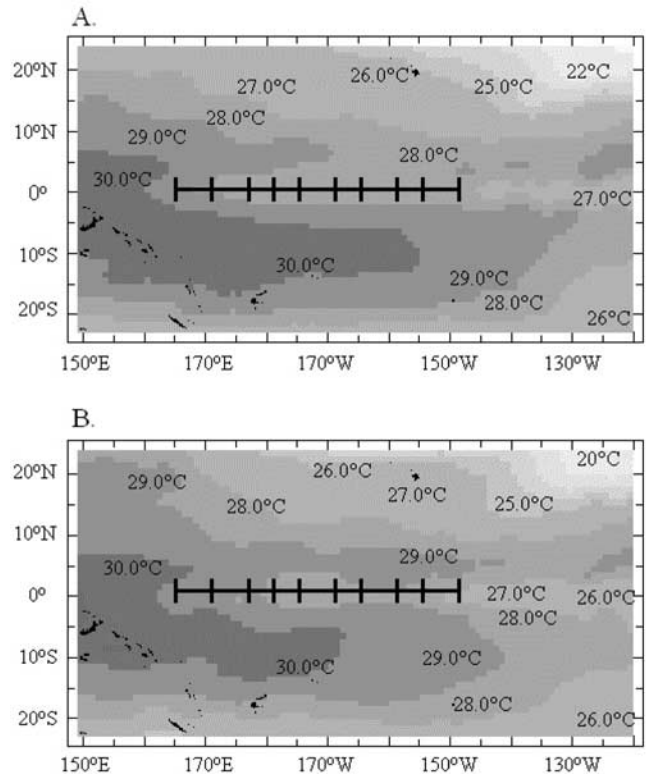


Figure 1. Weekly averaged Sea Surface Temperature (SST) for the (a) first and (b) last week of the six week cruise. The ship's track along equator is shown as a solid black line, tick marks indicate the station locations. SST images were produced by the LDEO Climate Group using satellite data provided by NESDIS and in situ data radioed from the Global Telecommunication System.

chlorophyll a (chl-a) fluorometer. Chl-a and phaeopigment concentrations in each sample were determined fluorometrically using a bench-top Turner Model 10-AU fluorometer [Holm-Hansen *et al.*, 1965]. Particulate absorption, a_p , was determined spectrophotometrically on samples filtered onto Whatman GF/F glass fiber filters. The average volume filtered was two and a half liters. Additionally, samples were fractionated, in parallel, into $<10 \mu\text{m}$, $<5 \mu\text{m}$ and $<3 \mu\text{m}$ fractions by prefiltering 5L of seawater through polycarbonate filters of the desired pore size prior to filtration onto Whatman GF/F glass fiber filters. Optical density of the particulate samples was measured in a Beckman UV-VIS 100 spectrophotometer over the wavelength range 350–800 nm within minutes of filtration. The reference filter, path amplification factor and uncertainty in absorption were handled according to Roesler [1998], with the small infrared offset removed [Babin and Stramski, 2002]. The phytoplankton and CPM absorption components (a_p and a_{CPM} , respectively) were obtained via extraction following Kishino *et al.* [1985] and Roesler and Perry [1995].

[9] In order to preserve closure between the particulate and dissolved fractions of the discrete samples and to gain a better understanding of CDOM composition, the GF/F filtrate was analyzed. Filtrate samples for CDOM absorption analyses were obtained from parallel filtrations

using Whatman GF/F filters (nominal pore size $<0.7 \mu\text{m}$) and $<0.45 \mu\text{m}$ and $<0.2 \mu\text{m}$ Gelman Supor-200 filters. These size-fractions will henceforth be denoted $a_{\text{CDOM}, <0.7}$, $a_{\text{CDOM}, <0.45}$, and $a_{\text{CDOM}, <0.2}$, respectively. Multiple rinses of glassware and filters and minimal handling were employed to ensure cleanly collected samples. Samples were stored in acid rinsed 50 ml amber borosilicate bottles, capped with Teflon-lined closures and kept frozen for later laboratory analysis. While freezing samples is not an ideal protocol, it is preferable to refrigeration [Hoge *et al.*, 1993] to minimize microbial activity, and may be necessary when accurate spectrophotometric measurements cannot be performed at sea. Storage effects, if any, would be systematically observed over the entire sample set. While differences in the magnitude of absorption measured in situ and spectrophotometrically were found, the same pattern in the spatial distributions of CDOM absorption were reflected in both sets of observations. CDOM optical densities were measured in a Cary 3E UV-VIS spectrophotometer over the wavelength range of 200–850 nm in 10-cm quartz cuvettes using 0.2 μm -filtered MilliQ water as the reference medium. Equivalent temperatures in sample and reference cuvettes were maintained to minimize absorption errors associated with the temperature dependence of water absorption at the red wavelengths [Pegau and Zaneveld, 1993]. The absorption coefficient for the size fractionated CDOM samples, was obtained as described by Bricaud *et al.* [1981].

2.2. In situ Measurements

[10] In situ profiles of conductivity, temperature, absorption and attenuation were conducted independently, following the hydrocasts. In situ IOPs were measured using a slightly negatively buoyant optical instrumentation package that included a SeaBird SBE-25 CTD and two WET Labs nine-wavelength absorption and beam attenuation meters (ac-9). IOPs derived from ac-9 measurements are calibrated relative to pure water and thus represent the absorption by the particulate and dissolved components only. Hereafter the measured total absorption, $a_T(\lambda)$, implies the sum of particulate and dissolved materials.

[11] The intake ports of all the ac-9 absorption and beam attenuation flow tubes were co-located to ensure comparable measurements. A 0.2- μm Gelman Supor-100 filter capsule was affixed to the intake port of one ac-9 absorption flow tube to obtain in situ CDOM absorption profiles, a_{CDOM} . The ac-9 measurements were corrected for temperature [Pegau *et al.*, 1997] then scattering [Bricaud *et al.*, 1995b; Roesler, 1998]. The instrument resolution is 0.005 m^{-1} . Spectral scattering coefficients, b_T , were derived by subtracting a_T from the concurrently measured total beam attenuation coefficients, c_T . Particulate absorption, a_p , was obtained by subtracting the corresponding a_{CDOM} from a_T . Particulate attenuation, c_p , was obtained by subtracting the corresponding a_{CDOM} from c_T .

2.3. Modeled Phytoplankton and CPM Spectra

[12] The relative contributions of major light-absorbing components were retrieved from the ac-9 a_T via in situ filtration and decomposition. The a_{CDOM} was measured directly by an ac-9. The a_p was decomposed into estimates

of phytoplankton, \hat{a}_ϕ , and CPM, \hat{a}_{CPM} , absorption using the full spectral model developed by Roesler *et al.* [1989]. In this case, the decomposition of multispectral ac-9 measurements of a_T minus the a_{CDOM} spectrum, measured by the second ac-9, will yield \hat{a}_ϕ , and \hat{a}_{CPM} . Input parameters for the model were the exponential slope of the CPM absorption spectrum (S_{CPM}) and blue-to-red phytoplankton absorption peak ratio, ϕ . A constant value of 0.011 was used for S_{CPM} , characteristic of detrital material or adsorbed labile humic acids [Carder *et al.*, 1989; Roesler *et al.*, 1989]. The blue-to-red absorption peak ratio for phytoplankton, ϕ , of 1.8 was corrected for the average observed phaeophytin-to-chl-a ratio [Roesler *et al.*, 1989]. A promising alternative parameterization was explored to test the blue-to-red peak parameter in the original model because there is a definite concern that the fluorometrically derived phaeopigment measurement might be affected by the presence of chlorophyll-b in these waters [Lorenzen and Downs, 1986; Welschmeyer, 1994]. This alternative parameter derives a blue-to-red peak ratio, ϕ , based on open ocean phytoplankton spectra and is dependent only on measured chl-a concentrations, where $\phi = 2.019 * [\text{chl a}]^{-0.173}$, following the model of Bricaud *et al.* [1995a]. The results with the alternate parameter yielded a model solution that slightly overestimates the discrete sample a_ϕ at 440 nm with a tendency for \hat{a}_{CPM} at 440 nm to be negative. A least squares fit, $y = ax$, to the modeled versus discrete sample a_ϕ at 440 nm yielded slopes of $a = 1.36$ for the model with the alternate parameter. The original parameterization of the model reproduced the discrete sample a_ϕ at 440 nm, yielding a nearly 1:1 relationship ($a = 0.98$). On the basis of these results, the Roesler *et al.* [1989] model is validated for this data set using a constant value for the blue to red peak absorption ratio of 1.72.

[13] The analysis conducted in this investigation carefully separates the use of discrete sample and in situ (ac-9) measurements. While we find that the distributional patterns of absorption measured in situ and from discrete samples were the same, the magnitudes of the coefficients were different (detailed below). Thus data interpretation involving comparisons between the two approaches required nondimensionalization of one set of measurements. Because of inherent uncertainties associated with sample handling in discrete sample analyses, we use these observations for distributional analyses, rather than absolute magnitudes.

2.4. Water Mass Analysis

[14] A multiple regression analysis based on methods by Thompson and Edwards [1981] and Mackas *et al.* [1987] is used to further characterize the conservative behavior of the light-absorbing components. This analysis is useful because ideally conservative tracer behavior can be compared to observations and the accuracy of the characterization of the water types can be assessed. Any passive tracer may be used (e.g., chl-a and nutrients), but this analysis focuses on the behavior of inherent optical properties. This simple analysis aids interpretation of variable distributions in two spatial dimensions. The effects of advection and/or propagating signals such as waves cannot be detected by this analysis, nor mixing from a third dimension. This type of analysis assumes water types are mixing along isopycnals or are able

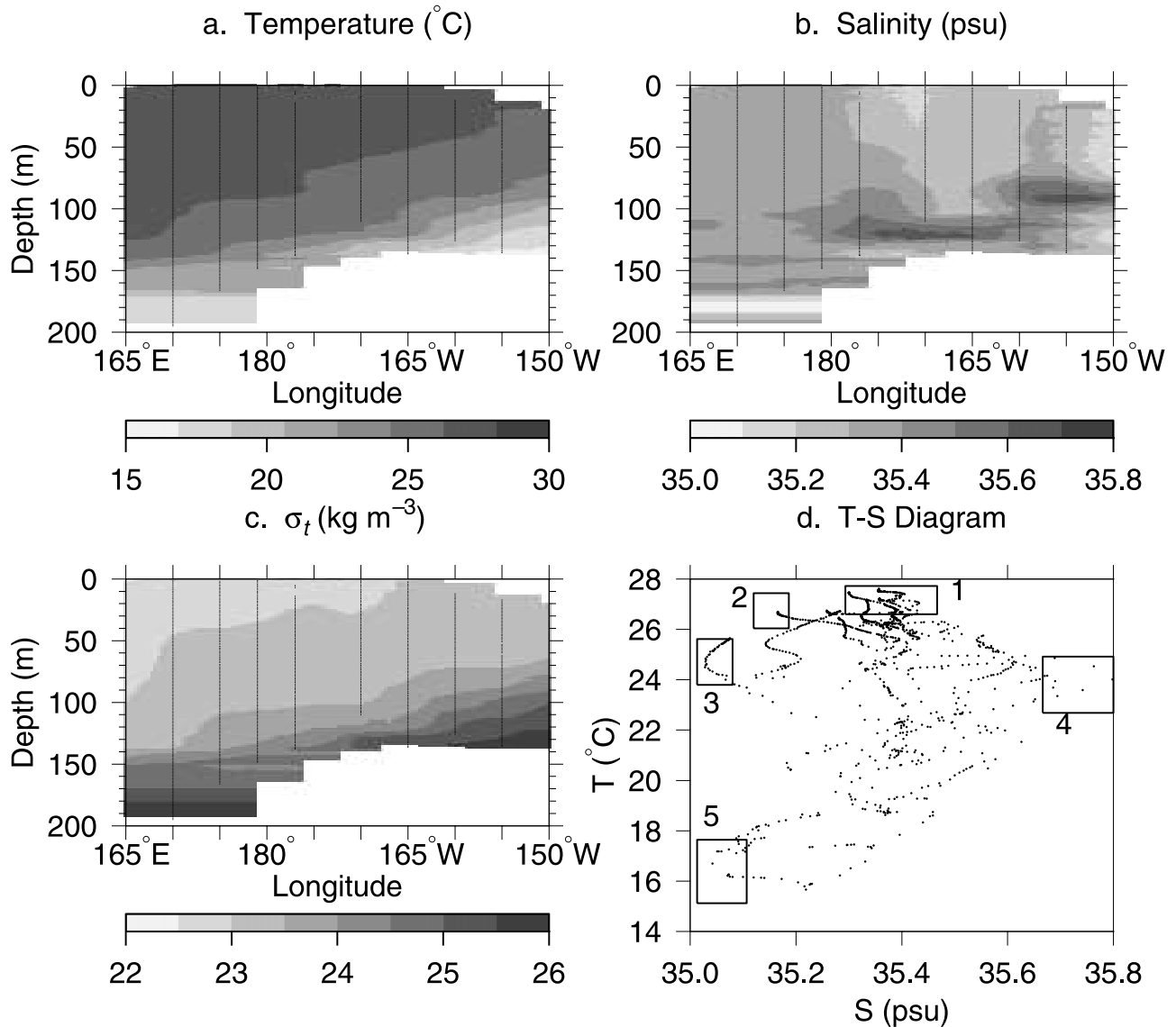


Figure 2. Vertical sections of (a) temperature, (b) salinity and (c) σ_t . Profile locations are marked by a continuous line of bullets. (d) The T-S diagram for the equatorial transect, with five water types identified. Observable are the probable water mixtures, M1 and M2.

to mix in a linear fashion. The multiple linear regression method solves the Normal equations having the form, $Py = u$. P is a matrix of hydrographic and optical properties of the source water types. Then, y is the solution vector that returns the fractional contributions of the source water types to the mixture. The vector, u , contains the hydrographic and optical properties of the mixture given y .

[15] In the forward use of the regression, representative values for hydrographic and optical properties are used to construct P . The fractional contributions of source water types, y , were assumed. Solving the system yields the ideally conservative hydrographic and optical properties of the resultant mixture, \hat{u} . The inverse application of the regression analysis requires the construction of P as stated for the forward model, but now mixture observations, u , are input, and the solution, \hat{y} , is subjected to a constraint that the sum of the elements in y are equal to one and that the elements are nonnegative, as negative water type

contributions are unrealistic. The system is then solved for the theoretical fractional contribution of source water types, \hat{y} .

3. Results

3.1. Hydrography

[16] The weekly averaged sea-surface temperature (SST) images of the first and last week of the cruise (Figure 1) show the cold tongue of upwelled water along the equator and the tendency for the SEC and ECC to become increasingly warm at the western end and north of the transect during the cruise period. In situ temperatures were maximal in the surface waters at the western end of the transect (28°C) and minimal at 150 m depth at the eastern end (15.5°C). The isotherms shoaled progressively toward the east (Figure 2). Salinity ranged from approximately 35.0 to 35.75 psu along the transect, with a mean of 35.34 psu

Table 1. Range of Hydrographic Parameters for Five Identified Water Types Along the Equator (165°E to 150°W)

| Water Type | T, °C | Salinity, psu | σ_t , kg m ⁻³ |
|------------|-----------|---------------|---------------------------------|
| T1 | 27.0–28.0 | 35.30–35.43 | 22.72–22.97 |
| T2 | 26.0–27.0 | 35.15–35.21 | 22.88–23.15 |
| T3 | 24.0–26.0 | 35.04–35.10 | 23.11–23.67 |
| T4 | 23.0–25.0 | 35.60–35.80 | 23.95–24.39 |
| T5 | 15.0–18.0 | 35.05–35.30 | 25.50–26.01 |

(Figure 2b). A plume of low salinity water extended from the surface at 170°W to nearly 100 m at 165°W. A regional maximum of higher salinity water was located between 177°W and 155°W at 100–120 m. The density structure of the upper water column was thermally driven, with the exception of very low salinity water at 170°W (Figure 2c). On the basis of the T-S diagram, we identified five distinct water types and two distinct water mixtures along the transect (Figure 2d). The five types, denoted T1 to T5, are delineated in Figure 2d. The two mixtures, M1 and M2, are observable as the diapycnally mixing portions in the T-S diagram. The range of magnitudes of the hydrographic properties of each type and mixture are shown in Table 1.

[17] T1, a deep, warm, saline, mixed layer was located at 165°E and shoaled eastward. T2, also warm, but fresher than T1, was located in the upper 40 m at 170°W. T3 formed the relatively fresher layer between 50 and 100 m at 150°W. T4, the most saline of the identified water types, was found at depth (80 to 140 m) east of the dateline, eventually venting at the eastern end of the transect. T5, significantly fresher and cooler than T4, was found beneath T4 between 165°E and 170°E ($z > 165$ m) and again between 155°W and 150°W ($z > 140$ m). Water mass M1 results from the diapycnally mixing between the source water types T1, T2, T3, and T4, and comprises most of the water column above 100 m. M2 results from diapycnally mixing across a small range of isopycnals between T4 and T5 and follows the base of the pycnocline.

3.2. Spatial Distributions of Inherent Optical Properties

[18] The magnitudes of b_T and a_T at 440 nm displayed more vertical than zonal variation, with maximal values above 100 m (Figure 3). This vertical variation was also observed during the JGOFS-FLUPAC cruise [Dupouy *et al.*, 1997]. Not surprising, the spatial distribution of a_T was more similar to the chl-*a* distribution than to b_T . The b_T maximum was shallower than the a_T maximum; as is commonly observed [Kitchen and Zaneveld, 1990].

[19] The shapes of particle attenuation spectra were relatively invariant throughout the region, displaying a hyperbolic spectral slope, γ , of the form:

$$c_p(\lambda) = c_p(440) \left(\frac{\lambda}{440} \right)^{-\gamma}$$

where λ is wavelength and the derived γ values were 1.00 ± 0.23 . The observed γ values indicate steep Junge distributions for particle size, suggesting dominance by small particles [Boss *et al.*, 2001].

[20] The distribution of a_{CDOM} at 440 nm, as measured with the ac-9, shows the relatively low magnitudes in the upper water column and large magnitudes in the deeper waters below the pycnocline (Figure 4a). Exceptions to this distribution occurred at 177°W, where larger magnitudes were observed throughout the water column, a feature that may have been caused by a recent upwelling event as evidenced by hydrographic (i.e., salinity) properties. Large values were also observed throughout the water column at 150°W. In general, above the pycnocline, a_{CDOM} contributed about 45% to a_T , while below the pycnocline the percentage was closer to 80%, consistent with the observations made by Siegel *et al.* [2002].

[21] Analysis of the size fractionated discrete CDOM samples indicated that there was no significant difference in absorption between the <0.45- and the <0.7- μm filtrates indicating that all the variation was in the <0.2 and the 0.2 to 0.45 μm ranges. However, for closure with the discrete particulate samples we will use the <0.2 and the 0.2 to 0.7 μm ranges (Figures 4b and 4c). Like the a_{CDOM} measured with the ac-9, the $a_{CDOM, <0.2}$ was dominant in deep waters, and at the 177°W upwelling site. A subsurface maximum in the 0.2 to 0.7 μm CDOM absorption, $a_{CDOM, 0.2-0.7}$, was observed in the upper 50 m of the water column, particularly at 177°W and at the easternmost station at 150°W. Larger magnitudes of $a_{CDOM, 0.2-0.7}$ were also associated with T4 at 100 m depth.

[22] A comparison of the <0.2 μm CDOM absorption distributions derived from in situ and discrete observations indicates no correlation between the <0.2 μm fractions

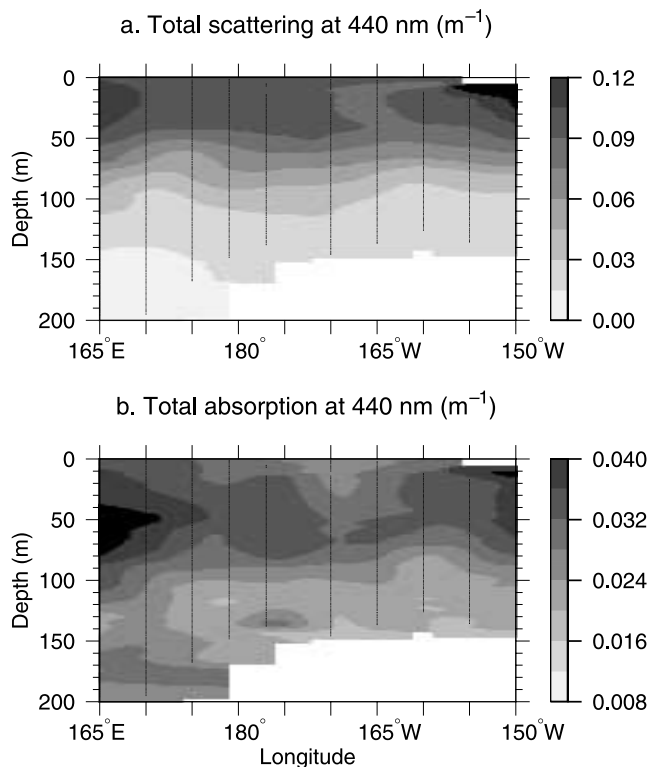


Figure 3. Vertical distributions of (a) total scattering coefficient at 440 nm and (b) total absorption at 440 nm along the equatorial transect. Profile locations appear as a continuous line of bullets. Note different scales on panels.

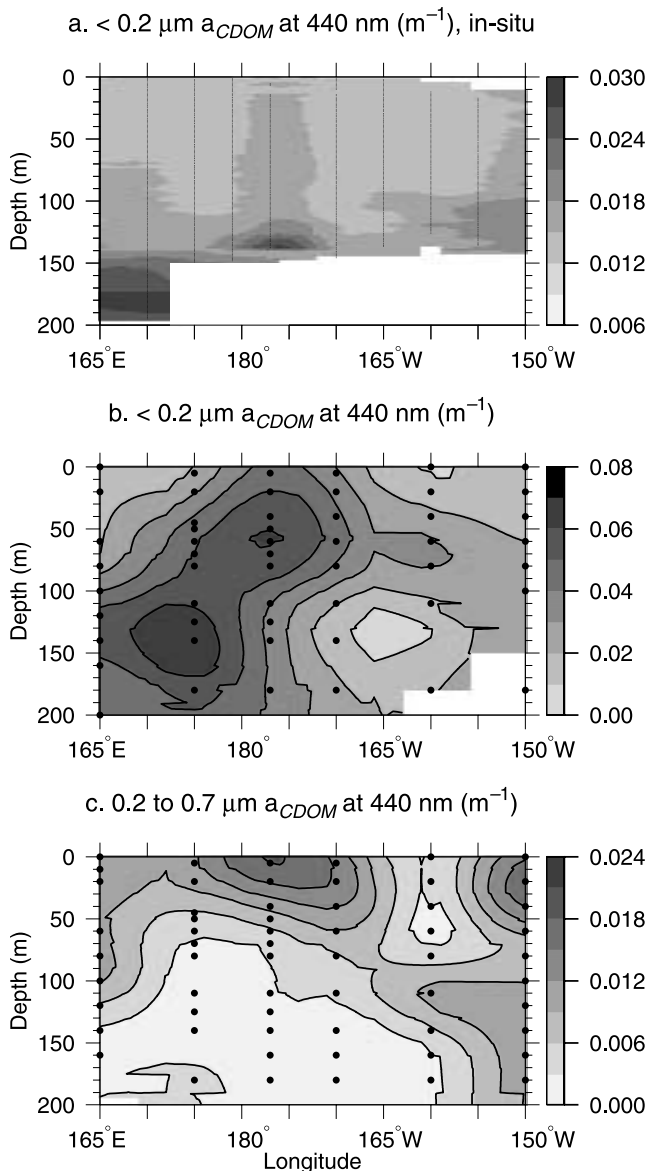


Figure 4. Vertical sections of CDOM at 440 nm: (a) $<0.2 \mu\text{m}$ CDOM absorption measured in situ with a filtered ac-9, (b) discrete sample $<0.2 \mu\text{m}$ CDOM absorption and (c) discrete sample $0.2 \text{ to } 0.7 \mu\text{m}$ CDOM absorption. Bullets indicate data locations.

($r = -0.045$, $\rho_{\text{crit}} = 0.3193$ at the 95% confidence level). However, once the distribution of the $0.2 \text{ to } 0.7 \mu\text{m}$ fraction is included, the spatial distributions are much more similar, particularly at 177°W and 150°W . This suggests that the efficiencies of the in situ filter cartridge versus the flat round filter disc are somewhat different and that the in situ observations made with the $0.2\text{-}\mu\text{m}$ filter were comparable to the discrete observations made with the $0.2\text{-}\mu\text{m}$ filter plus some portion of the $0.2 \text{ to } 0.7\text{-}\mu\text{m}$ fraction. The difference in absolute values between the ac-9 and discrete sample observations shows an underestimation by the ac-9 (or overestimation in the discrete samples) by approximately a factor of one half outside the upwelling signature. It has been previously documented that discrepancies of $>25\%$ and RMS values of 0.045 m^{-1} are found between laboratory

spectrophotometers and reflecting-tube absorption meters [Pegau *et al.*, 1995; Pegau, 1997]. The deviation has been attributed to the instrument configurations, insensitivity of the ac-9 detectors in the blue region, as well as sample collection methods and spatial resolution and heterogeneity between casts. There exists the added degree of uncertainty given that the discrete analyses were performed on frozen samples. The impacts of freezing on these samples were not possible to verify, but unpublished data show $<10\%$ difference between fresh and frozen samples obtained from coastal waters. Given the statistic, the CDOM absorption measured via either method yield the similar information on the spatial distribution of this variable and the size fractionation provides more information about source and type of CDOM. For the purposes of this investigation, the relative distributions and normalized (nondimensional) spectra of the size-fractionated discrete sample CDOM measurements are used for interpretation.

[23] CPM absorption (\hat{a}_{CPM}) at 440 nm was $<0.01 \text{ m}^{-1}$ throughout the region (Figure 5a), comparable to values observed in this region on other cruises [Allali *et al.*, 1997; Dupouy *et al.*, 1997]. On average, \hat{a}_{CPM} at 440 nm contributes about 20% of $a_p(440)$ and 11% of $a_T(440)$ above the pycnocline. Bricaud *et al.* [1998] calculated ratios of $a_{\text{CPM}}:a_p$ ranging between 0.01 and 0.1 during the OLIPAC and FLUPAC cruises. Dupouy *et al.* [2003] estimated values of $a_{\text{CPM}}:a_T < 0.14$ for this region. This suggests that the modeled CPM may be slightly overestimated, but is generally in the range of published values. The correlation between the modeled and discrete sample a_{CPM} is weakly positive, but significant ($r = 0.324$, $\rho_{\text{crit}} = 0.2701$ at the 95% confidence level). The poor correlation may be due to the extremely low values of a_{CPM} , which fall to the level of the ac-9's resolution threshold. Size fractionated CPM absorption was negligible or not detectable. This does not imply the absence of nonalgal particulates because these materials are likely weakly absorbing [DuRand and Olson, 1996; Claustre *et al.*, 1999; Simeon, 2001; Bricaud *et al.*, 2002].

[24] The distribution of phytoplankton absorption (\hat{a}_ϕ) at 440 nm also demonstrated more vertical than zonal variation (Figure 5b). The largest magnitudes were found in the upper 100 m, especially at the easternmost and westernmost portions of the transect. On average, \hat{a}_ϕ at 440 nm contributed 86% of $a_p(440)$ and 39% of $a_T(440)$. The >10 , 3 to 10, and $<3 \mu\text{m}$ phytoplankton size classes respectively contributed on average 7%, 15% and 78% of the total phytoplankton absorption. The comparison of modeled and discrete sample phytoplankton absorption at 440 nm exhibited a strong positive correlation, significant at the 95% confidence level ($r = 0.773$, $\rho_{\text{crit}} = 0.287$ at the 95% confidence level).

[25] The distribution of chl-a (Figure 5c) along the equator exhibited a subsurface maximum at 50 m that extended from 165°E to 170°W then shoaled to 25 m between 160°W and 150°W . Chl-a concentrations within the maximum ranged between $0.35 \text{ to } 0.40 \text{ mg m}^{-3}$. Concentrations of $0.1 \text{ to } 0.2 \text{ mg m}^{-3}$ were found in the upper 40 m of the water column between 177°W and 165°W . Below 100 m, concentrations were less than 0.1 mg m^{-3} .

[26] To summarize, the distributions of component absorption indicate major contributions by CDOM and phytoplankton. This is consistent with measurements made by

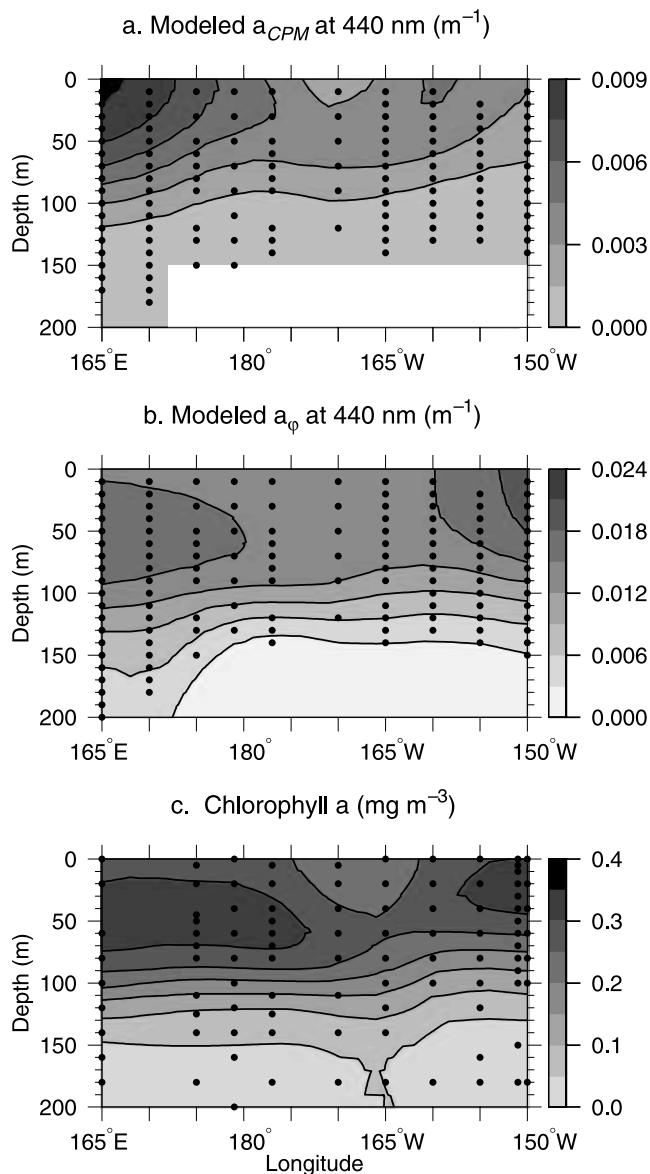


Figure 5. Modeled (a) CPM absorption, (b) phytoplankton absorption and (c) chlorophyll-a concentrations. Bullets indicate data locations. Note different scales on panels. See text for further details of model.

Parslow et al. [1998]. Variations in a_T above 100 m were primarily due to variations in \hat{a}_ϕ , except at 177°W , where amplified a_{CDOM} values were observed throughout the water column. Below 100 m a_T was due predominantly to a_{CDOM} . The spectral slope of particulate attenuation indicated a particle size distribution dominated by small particles, which is consistent with the results of the size-fractionated phytoplankton absorption.

3.3. Water Type Optical Properties

[27] The IOP means and standard deviations within each water type identified in the T-S diagram were estimated (Table 2) from the in situ observations. F tests for the equality of sample variances at the 95% confidence level were applied to determine the significance of the inherent optical property values associated with each water type

(Table 3). The F -test hypothesis is that the sample variances are the same. The results of the F -tests show that $b_T(440)$ in T1, T2 and T3 are significantly different from $b_T(440)$ in T4 and T5. The in situ $<0.2 \mu\text{m } a_{\text{CDOM}}(440)$ found in T1, T2 and T3 were all significantly different from each other, but deep water values from T4 and T5 were not significantly different from any of the values found in other water types. This suggests that the a_{CDOM} originating from deep water is ubiquitous, likely a result of the high values in the upper water column at 177°W and 150°W . The $\hat{a}_\phi(440)$ found in T1 was significantly different from the $\hat{a}_\phi(440)$ found in other water types. The $\hat{a}_{\text{CPM}}(440)$ found in T1, T3 and T4 were significantly different from each other.

4. Discussion

4.1. Water Types and Mixtures

[28] The observations of hydrographic and optical properties were recorded over a four-week period. Aliasing in the measurements is minimized as the South Equatorial Current (SEC) propagates westward during La Niña conditions. The weekly integrated SST images of the first and last week of sampling indicate that SEC water masses were warmed toward the east along with the Equatorial Counter Current (ECC), north of the transect. The cold tongue propagated westward with the SEC1 south of the transect. Along the equator, the upwelling weakened in the west and strengthened in the east. The σ_t structure of the water column was thermally driven by the influx of solar radiation and the outcropping cold deep waters.

[29] Hydrographic characteristics were used to identify distinct water types along the transect. The hydrography revealed the presence and positions of the SEC, Equatorial Undercurrent (EUC) and Equatorial Intermediate Current (EIC). The SEC was located in the upper water column along the transect. T1, T2 and T3 were distinct water types within the SEC. Salinity permits further distinction of the SEC's northern (SEC1) and southern (SEC2) branches. The hydrographic characteristics of T1 corresponded to the characteristics of the SEC1 [*Wyrski and Kilonsky, 1984; Carr et al., 1992*]. The SEC2 was associated with the cold tongue from the east. T2, distinguishable because of its relatively lower salinity, matched previously published hydrographic characteristics of the SEC2 [*Wyrski and Kilonsky, 1984; Carr et al., 1992*]. The possibility that intense rainfall caused the relatively fresher salinity signature of T2 would require an introduced volume of rainwater on the order of 40 cm of precipitation. T3 was likely another parcel of the SEC2.

[30] The most saline water mass, T4, found below 120 m, was likely transported by the EUC. A high vertical shear

Table 2. Mean \pm Standard Deviations of Component Absorption at 440 nm (m^{-1}) for the Five Water Types^a

| Water Type | $a_{\text{CDOM}} < 0.2 \mu\text{m}$ | \hat{a}_ϕ | \hat{a}_{CPM} |
|------------|-------------------------------------|-------------------|------------------------|
| T1 | 0.013 ± 0.001 | 0.015 ± 0.002 | 0.009 ± 0.002 |
| T2 | 0.012 ± 0.001 | 0.013 ± 0.001 | 0.001 ± 0.002 |
| T3 | 0.016 ± 0.001 | 0.021 ± 0.001 | 0.002 ± 0.001 |
| T4 | 0.019 ± 0.003 | 0.003 ± 0.003 | 0.000 ± 0.000 |
| T5 | 0.025 ± 0.004 | 0.004 ± 0.003 | 0.000 ± 0.000 |

^aThe size fraction for a_{CDOM} is $<0.2 \mu\text{m}$. $N = 15$ for each mean.

Table 3. Results From F-Tests for the Equality of Sample Variances in Water Types^a

| | $b_T(440)$ | | | | | $<0.2 \mu\text{m } a_{\text{CDOM}}(440)$ | | | | | $\hat{a}_\phi(440)$ | | | | | $\hat{a}_{\text{CPM}}(440)$ | | | | |
|----|------------|----|----|----|----|--|----|----|----|----|---------------------|----|----|----|----|-----------------------------|----|----|----|----|
| | T1 | T2 | T3 | T4 | T5 | T1 | T2 | T3 | T4 | T5 | T1 | T2 | T3 | T4 | T5 | T1 | T2 | T3 | T4 | T5 |
| T1 | | R | R | R | R | | R | R | A | A | | R | R | R | R | | A | R | R | A |
| T2 | R | | A | R | R | R | | R | A | A | R | | A | A | A | A | A | A | A | A |
| T3 | R | A | | R | R | R | R | | A | A | R | A | | A | A | R | A | A | R | A |
| T4 | R | R | R | | A | A | A | A | | R | R | A | A | | R | A | R | | | A |
| T5 | R | R | R | A | | A | A | A | R | | R | A | A | A | A | A | A | A | A | A |

^aThe hypothesis is that sample variances are the same: R, reject hypothesis; A, accept hypothesis.

zone associated with the rapid EUC appeared to be positioned between 130 to 140 m during the cruise. This was also evidenced by the optical package's occasional inability to penetrate into the deeper water column. The densest water mass, T5, had the salinity, temperature and position of the EIC and was discernible at station locations 165°W, 155°W and 150°W.

[31] The diapycnally mixed M1 was located between the SEC and EUC. An apparent front at 177°W is an obvious example. The temperature and σ_t structure around the dateline suggests instabilities at the front. At the front, steep salinity gradients are also observed. The other mixture, M2, occurs at the EUC/EIC interface. The steep density gradients and high shear limit this mixture to motion along a small range of isopycnals.

4.2. Conservative Behavior of Optical Components

[32] The conservative behavior of component absorption was determined with respect to the hydrography. A conservative tracer that is stable over time becomes an inherent property of a defined water mass. A conservative tracer of a distinct water mass, upon mixing with other water masses, will be linearly diluted. A regression analysis of a tracer against density would reveal the degree of control diffusive, mixing and/or advective processes have over the distribution of a passive tracer. Regressing both $b_T(440)$ and $a_T(440)$ onto σ_t yields correlations of $r = -0.71$ ($\rho_{\text{crit}} = 0.179$ at the 95% confidence level) and -0.62 ($\rho_{\text{crit}} = 0.179$ at the 95% confidence level), respectively. Regressions of $<0.2 \mu\text{m } a_{\text{CDOM}}(440)$, $\hat{a}_\phi(440)$ and $\hat{a}_{\text{CPM}}(440)$ onto σ_t respectively yield correlation coefficients of 0.63, -0.75 and -0.56 ($\rho_{\text{crit}} = 0.179$ at the 95% confidence level). The significant correlations indicate that physical processes have a fairly strong influence on IOP distributions (Table 4).

[33] A two-dimensional water mass analysis, a regression model, was used to determine the conservative variability due to mixing in the spatial distributions of hydrographic and optical properties. In the forward use of the regression, representative values for hydrographic and optical properties found in Tables 1 and 2 were used to construct the matrix, P, as described in section 2.4.

[34] Given a variety of fractional contributions by T1, T2, T3 and T4 to M1 in the forward model, frequency distributions of conservatively mixing IOPs can be predicted. The predicted frequency distributions of $b_T(440)$, ac-9 $<0.2 \mu\text{m } a_{\text{CDOM}}(440)$, $\hat{a}_\phi(440)$ and $\hat{a}_{\text{CPM}}(440)$ are compared with the respective frequency distributions of M1 observations (Figure 6). Note that observations from source water types are excluded from the frequency distributions of observed values. At first glance the observed absorption components appear to closely follow the predicted distribution. The model hindcast skill, significant at the 95% confidence level, shows

that 42% of the spatial variability in $b_T(440)$ in M1 can be ascribed to along-isopycnal mixing. The hindcast skill for the M1 $<0.2 \mu\text{m } a_{\text{CDOM}}(440)$, $\hat{a}_\phi(440)$ and $\hat{a}_{\text{CPM}}(440)$, show that 39%, 87% and 57% of the spatial variability, respectively in these components, is explained by along-isopycnal mixing. This result suggests that the spatial variability in $\hat{a}_\phi(440)$ and $\hat{a}_{\text{CPM}}(440)$ is strongly influenced by physical processes (mixing and/or diffusion). The regression analysis for the M2 mixture was inconclusive as only a small number of data could be obtained.

[35] The inverse model indicates that T1 and T5 are the most distinct water types contributing to the water mixtures. The regression analysis showed ambiguous contributions by T2 and T4 to the water mixtures. Inputting observations from the profile at 177°W shows large fractional contributions by T4, and to a lesser degree, T5 at depth and T1 nearer the surface.

[36] The spatial locations where IOPs are behaving conservatively are displayed graphically by the predicted mixture magnitudes, together with the source water type properties, on a linearly interpolated grid (Figure 7, left panels). The spatial locations where the IOPs are behaving nonconservatively are displayed as the difference between the observed and predicted mixture magnitudes interpolated on identical grids (Figure 7, right panels). West of 180°, $b_T(440)$ has some nonconservative variation in the near surface, while east of 180°, the nonconservative variation is between 50–100 m. The $<0.2 \mu\text{m } a_{\text{CDOM}}(440)$ measured by the ac-9 exhibits nonconservative behavior, east of 170°W between 80–100 m and throughout the water column at 177°W. The $\hat{a}_\phi(440)$ and $\hat{a}_{\text{CPM}}(440)$ exhibit the most non-conservative behavior above 70 m, associated with the $a_{\text{CDOM}, <0.2 \mu\text{m}}$ at the deep-water frontal feature at 177°W and the deep $a_{\text{CDOM}, 0.2-0.7 \mu\text{m}}$ at 150°W, respectively. The conservative variability is spatially coherent with the distribution of total absorption while the nonconservative variation generally decreases zonally eastward toward the newly vented waters at 150°W.

4.3. Nonconservative Behavior of Optical Components

[37] The nonconservative variability in the optical properties of the water types and mixtures can be attributed to

Table 4. Correlation Coefficients (r) for the Regression of IOPs Onto Density (σ_t)^a

| IOP | r | ρ_{crit} |
|-----------------------------|---------|----------------------|
| $b_T(440)$ | -0.7074 | 0.1792 |
| $a_{\text{CDOM}}(440)$ | 0.6325 | 0.1792 |
| $\hat{a}_\phi(440)$ | -0.7516 | 0.1792 |
| $\hat{a}_{\text{CPM}}(440)$ | -0.5855 | 0.1792 |

^aThe 95% confidence level (ρ_{crit}) is given.

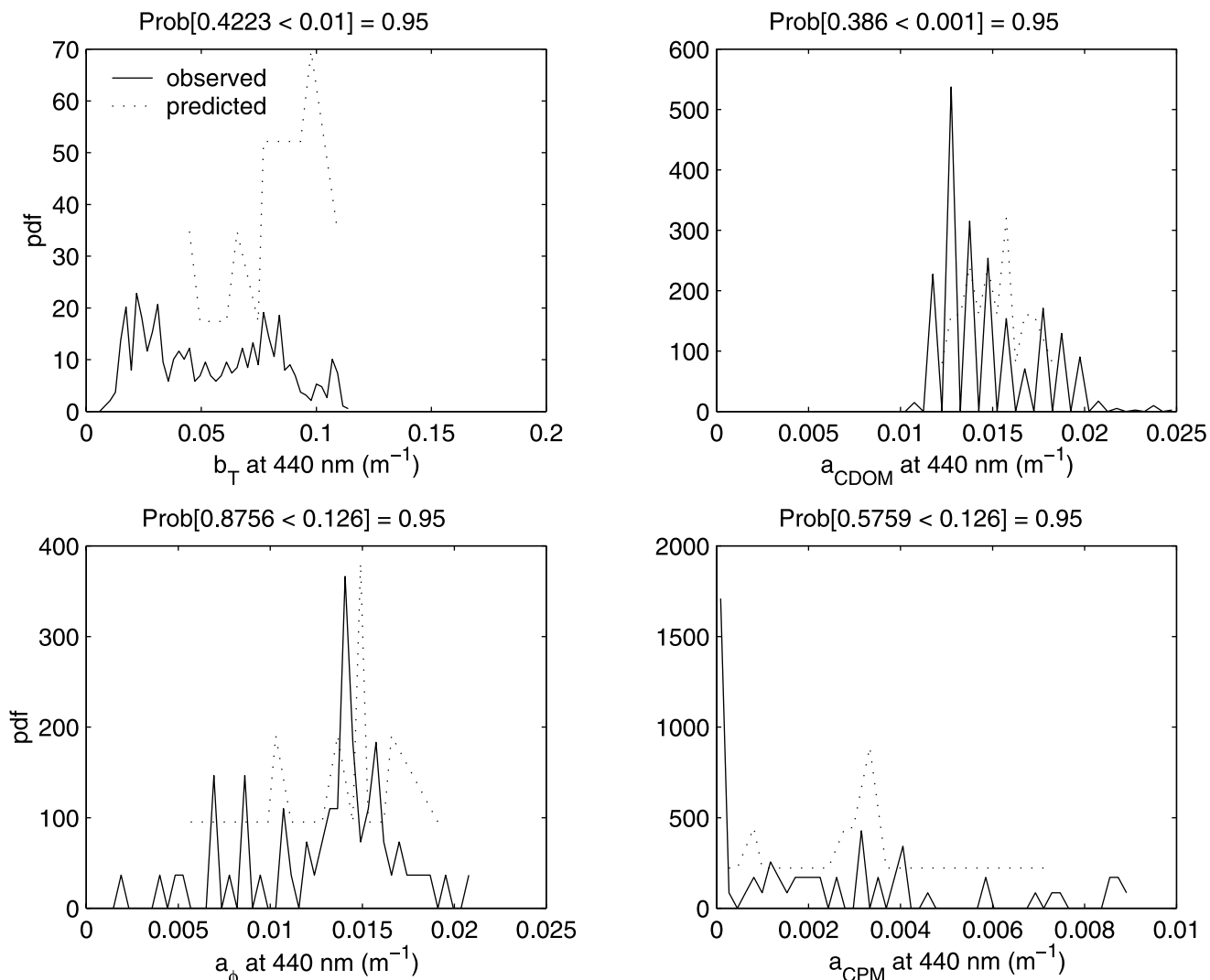
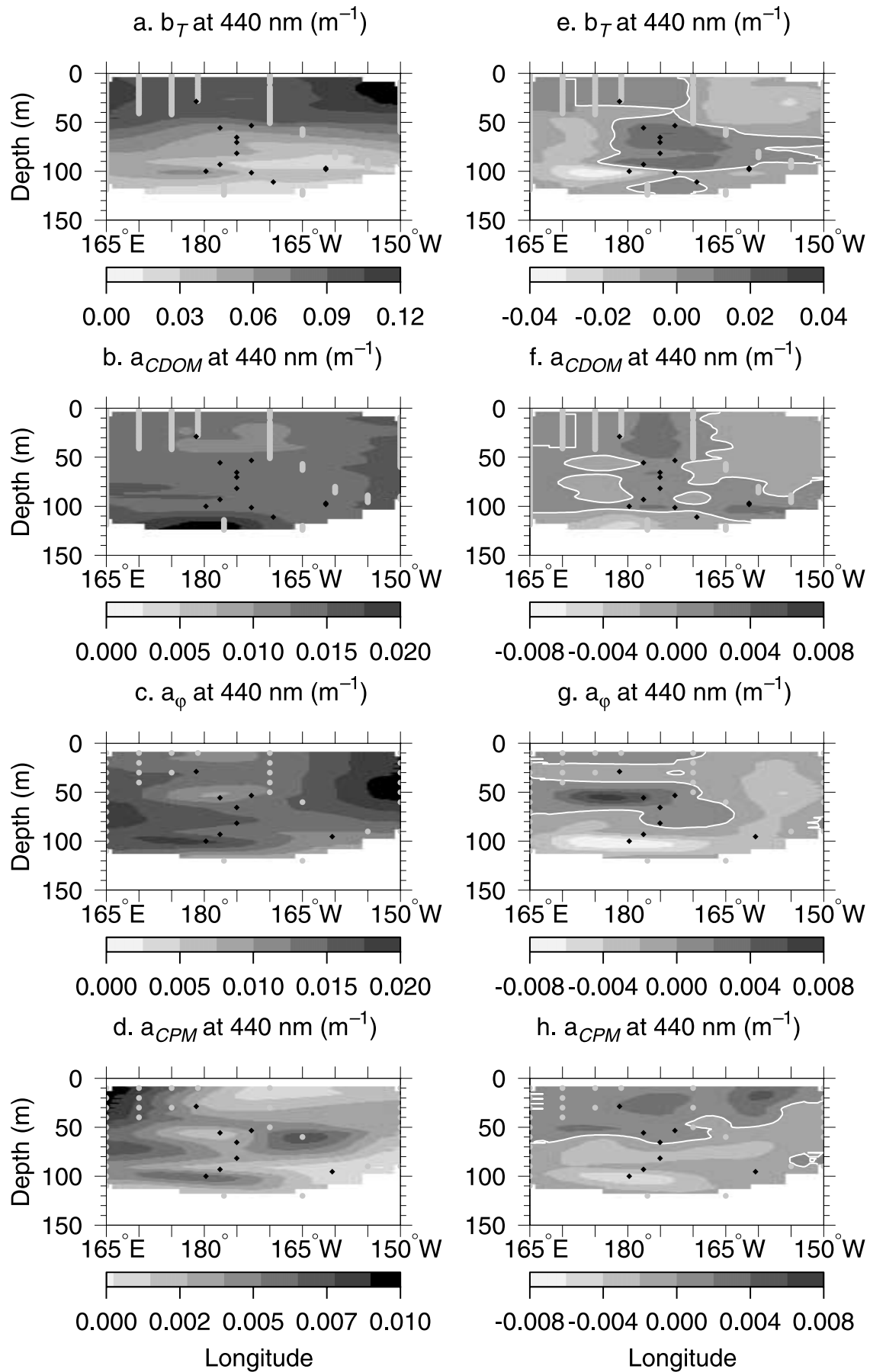


Figure 6. Probability distribution functions (pdfs) from the M1 water mass. Pdfs are created from M1 observations (solid) and predicted IOP values (dotted) given fractional contributions of source water types (T1, T2, T3 and T4). Clockwise from top, left: $b_T(440)$, $a_{CDOM}(440)$, $a_{CPM}(440)$, and $a_\phi(440)$. The hindcast skill of the regression model show $a_{CPM}(440)$ and $a_\phi(440)$ exhibit the most conservative mixing behavior at the 95% confidence level.

biogeochemical processes impacting the light-absorbing components [Siegel *et al.*, 1989; Mopper *et al.*, 1991]. Physical processes can explain only about half of the variance in the particulate scattering at 440 nm. It is of interest to note that the particulate scattering exhibited nearly uncorrelated variability patterns compared to the particulate absorption (i.e., depth versus zonal variation, respectively). Instead, the pattern of variability in particulate scattering was very similar to the pattern of nonconservative variability of $\hat{a}_\phi(440)$. This suggests that specific species of phytoplankton may be very important contributors to scattering within the phytoplankton absorption maxima.

[38] The particulate absorption components, $\hat{a}_\phi(440)$ and $\hat{a}_{CPM}(440)$, appeared to be strongly influenced by physical processes. The phytoplankton component exhibited stronger vertical versus zonal gradients, where zonal gradients in $\hat{a}_\phi(440)$ were largely conservatively varying. This is con-

firmed by examination of the scaled phytoplankton absorption spectra (scaled to the area under the curve to enhance variations in spectral shape by removing effects of biomass, [Roesler *et al.*, 1989]) as a function of longitude (Figure 8a) and a function of depth (Figure 8b). There was no evidence of zonal spectral variability, thus the nonconservative zonal variations are not due to changes in relative pigment absorption. There existed more variability in spectral shape observed as a function of depth, consistent with photoacclimation (Figure 8b, Harimoto *et al.* [1999]), particularly between 40 and 60 m. Dupouy *et al.* [2003] also found larger spectral variability in phytoplankton spectra below 60 m. The more minor zonal, nonconservative variation suggests that within the deeper mixed layers in the west, phytoplankton photoacclimation is a necessary strategy. The a_ϕ associated with different size fractions indicates that the nonconservative variations between 165°E and 165°W were due to the 3–10 μm fraction above 20 m, the <3 μm fraction



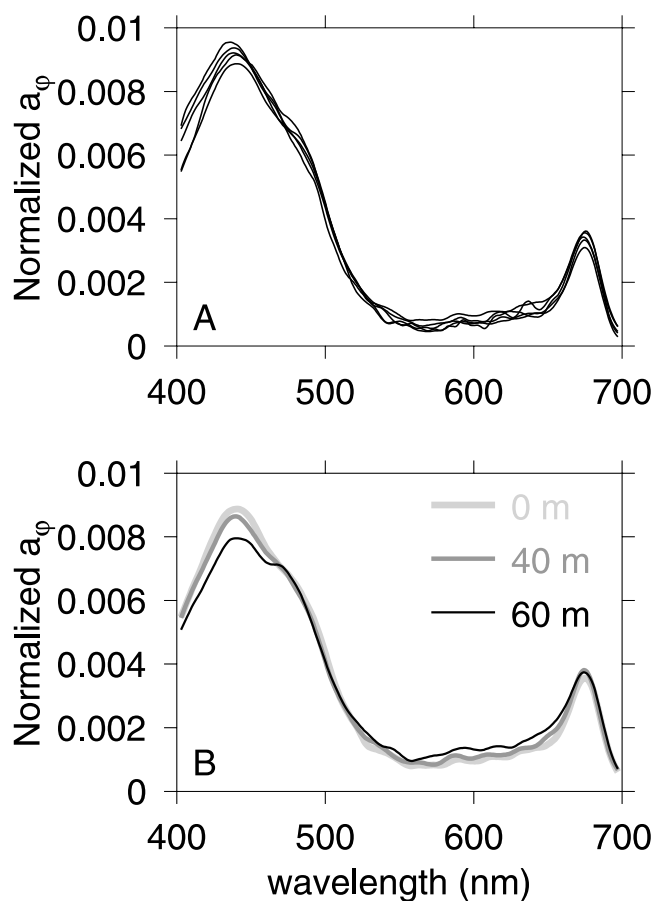


Figure 8. Normalized phytoplankton absorption spectra. (a) Spectra from surface samples across the transect at 175°E, 179°E, 177°W, 170°W, 160°W and 150°W. (b) Phytoplankton spectra from depths of 0, 40 and 60 meters at 160°W.

at 50 m, and the $>10 \mu\text{m}$ fraction at 80 m. Within the venting waters to the east, the physics and upwelling nutrients become the driving force. The sources of nonconservative variability in $\hat{a}_{\text{CPM}}(440)$ were difficult to identify given that this component was very weakly absorbing.

[39] The variability in $<0.2 \mu\text{m}$ $a_{\text{CDOM}}(440)$ was not wholly attributed to physical processes. While there is a fairly strong positive correlation between in situ observations of $a_{\text{CDOM}}(440)$ and σ_t , the mixtures did not completely support the role of physical processes in determining the a_{CDOM} distributions. The strongly absorbing CDOM at 177°W was likely recently upwelled from T4, where the dynamics of a front could permit the rapid vertical transport of the CDOM before photo-oxidation could completely bleach the signal. The nonconservative variation in a_{CDOM} indicated by the mixing model may be due to photo-oxidative effects of deep water CDOM. The discrete sample size fractions for CDOM showed the $a_{\text{CDOM}, <0.2}$ accounted

Table 5. Absorption Spectral Slopes, S_{CDOM} , for the <0.2 - and 0.2 to 0.7 - μm CDOM Fractions for the Five Water Types ($N = 7$, Standard Deviations are <0.001 for Each)

| Water Type | $S_{\text{CDOM}, <0.2 \mu\text{m}}$ | $S_{\text{CDOM}, 0.2 \text{ to } 0.7 \mu\text{m}}$ |
|------------|-------------------------------------|--|
| T1 | 0.014 | 0.011 |
| T2 | 0.011 | 0.011 |
| T3 | 0.013 | 0.011 |
| T4 | 0.013 | 0.013 |
| T5 | 0.013 | 0.013 |

for virtually all of the a_{CDOM} in deep waters, while above 50 m, the $a_{\text{CDOM}, 0.2-0.7}$ was equal to or exceeded $a_{\text{CDOM}, <0.2}$. [40] The nondimensional spectral shapes of the a_{CDOM} spectra yield information regarding the composition of CDOM [e.g., *Carder et al.*, 1989]. The exponential slope of the CDOM absorption, S_{CDOM} , for the two size fractions was examined within the five water types (Table 5). The spectral slopes of the $<0.2 \mu\text{m}$ CDOM were larger than those of the 0.2 to $0.7 \mu\text{m}$ fraction in T1 and T3, indicating different compositions of the chromophoric materials. Steeper spectral slopes were generally found in deep water CDOM of both fractions and the $<0.2 \mu\text{m}$ fraction throughout the water column.

[41] The analysis of the CDOM absorption spectral slopes demonstrates that the two size fractions were compositionally distinct, with steeper slopes found in the $<0.2 \mu\text{m}$ fraction and in the deep 0.2 to $0.7 \mu\text{m}$ fraction. Thus compositionally, the source of the $<0.2 \mu\text{m}$ CDOM fraction is likely to be from deep water. This is confirmed by variance tests applied to the water type CDOM, which indicates that the $<0.2 \mu\text{m}$ CDOM found throughout the water column was not significantly distinct from the deep water CDOM. The exact identity and source of these chromophoric dissolved materials are unknown and it is likely that the CDOM pool is a small subset of the DOM pool [*Nelson and Siegel*, 2002; *Siegel et al.*, 2002]. Other works perhaps aid the interpretation of the observed distributions [e.g., *Druffel et al.*, 1992; *Mopper and Schultz*, 1993; *Guo et al.*, 1995, 1996; *Skoog and Benner*, 1997; *Archer et al.*, 1997]. As described by these investigators, there exists a pool of low molecular weight organic compounds susceptible to photo-oxidation. This description coincides with the apparent properties of the $<0.2 \mu\text{m}$ CDOM fraction. This photosensitive fraction is said to be composed of old, refractory DOM. These relatively more refractory compounds are at least known to contain glucose and galactose [*Skoog and Benner*, 1997].

[42] Recent DOC concentration data have shown the tendency for an ephemeral pool of new DOC to concentrate at the sea surface [*Williams and Druffel*, 1987; *Druffel et al.*, 1992; *Guo et al.*, 1996; *Skoog and Benner*, 1997]. Though the 0.2 to $0.7 \mu\text{m}$ CDOM is a relatively smaller component of the CDOM, its concentration in the stratified, high-irradiance surface waters is indicative of a resistance to

Figure 7. (opposite) (left) The predicted mixture values (black diamonds) for M1 graphed with the end-member values (pale gray bullets) show the conservatively mixed distribution of IOPs. (right) The nonconservative absorption is quantified by subtracting the gridded, conservatively mixed distributions from the observed distributions on an identical grid. The symbols show the observed - predicted (black diamonds) and end-member (pale gray bullets, here are zero) data locations. The white curve marks the zero contour level.

photo-oxidation. The distribution of the 0.2 to 0.7 μm fraction within the upper 50 m also coincides with the location of increased biological activity associated with phytoplankton, so is likely of labile organic compounds and resistant to photo-oxidation. These characteristics of the 0.2 to 0.7 μm CDOM fraction are similar to properties of the described new DOM pool. The 0.2 to 0.7 μm CDOM in the upper water column likely consists of amino sugars, uronic acids, galactose and deoxysugars [Montgomery *et al.*, 1990; Mopper *et al.*, 1995; Skoog and Benner, 1997]. The 0.2 to 0.7 μm CDOM of the EUC and EIC was likely larger complexes of the same materials of the <0.2 μm CDOM since this signal shows up in the <0.2 μm CDOM measured by the ac-9 and has the steeper spectral slopes akin the deep <0.2 μm CDOM.

[43] As described by Archer *et al.* [1997], there exists the superimposed presence of the new and old DOM pools in the equatorial Pacific because of the strong upwelling. The separation of <0.7 μm CDOM absorption into size fractions and an analysis of their spectral slopes helps to resolve the superimposed presence of the new and old DOM pools. We surmise that the CDOM absorption at the surface was then caused by a combination of photo-oxidized deep water DOM and new DOM associated with phytoplankton, while the strong CDOM absorption in deep waters was due to the accumulation of older, refractory DOM. Given that the <0.2 μm fraction was responsible for most of the total CDOM absorption, this suggests most of the chromophoric dissolved materials in the equatorial Pacific are composed of older, low molecular weight, refractory organic compounds. These results are consistent with the conclusion by Siegel *et al.* [2002], that physical, photochemical and biological processes regulate the global distribution of CDOM and that the relative importance of each process has a directional dependence.

5. Conclusions

[44] The sources of spatial variability in component absorption along an equatorial Pacific transect are both physical and biogeochemical. The Zonal Flux cruise took place during mild La Niña conditions, where a “warm pool” to the west was contrasted by the cold tongue to the east. The hydrographic properties recorded during the cruise revealed the presence of five distinct water types and two general mixtures which were associated with major currents found at the equator: the SEC1, SEC2, EUC and EIC. A regression analysis showed that the statistically best optically characterized water types were associated with the SEC1 and the EIC.

[45] One source of spatial variability along the transect was due to physical mixing of water types above 100 m. The inherent optical property components all demonstrated significant correlations with density. The observed IOP magnitudes within the water mixture above 100 m displayed statistically significant similarities to predicted magnitudes given linear mixing of the identified water types. The mixing model assumes 2-D along isopycnal mixing and indicates that 42%, 39%, 87% and 57% of the spatial variability in $b_T(440)$, <0.2 μm $a_{\text{CDOM}}(440)$, $\hat{a}_\varphi(440)$ and $\hat{a}_{\text{CPM}}(440)$, respectively, is due to conservative mixing.

[46] The remaining variability in IOPs that is not attributable to physical processes is due to biogeochemical processes differentially acting on each component. For the phytoplankton component, the zonal variability in the subsurface chl-a and a_φ maxima is likely due to changes in biomass and to the rare presence of >3 μm cells that contributed as much as 22% to the total phytoplankton absorption. Photoacclimation is likely the source of vertical variations in phytoplankton absorption. The CPM absorption exhibits low magnitudes throughout the transect, but does not imply low concentrations of these materials because they tend to be weakly absorbing.

[47] A potential source of nonconservative variation in the <0.7 μm CDOM absorption is due to differing processes acting on two compositionally different pools of CDOM. The 0.2–0.7 μm fraction was found near the surface across the transect, above 50 m. The distribution of this fraction suggests these materials are labile organic compounds, resistant to photo-oxidation. The largest magnitudes of <0.2 μm a_{CDOM} were found below 150 m. An upwelling event of deep CDOM contrasts with the low magnitudes of <0.2 μm CDOM above 150 m and suggests the photosensitivity of this fraction. The characteristics displayed by these two fractions strongly indicate the superimposed presence of the new and old DOM pools described by Archer *et al.* [1997].

Notation

| | |
|--|--|
| a_{CDOM} | absorption coefficient of chromophoric (colored) dissolved organic matter, m^{-1} . Size fractions may also be denoted in the subscript. |
| $a_{\text{CPM}}, \hat{a}_{\text{CPM}}$ | measured and modeled, respectively, absorption coefficient of chromophoric (colored) particulate matter, excluding in vivo phytoplankton pigments, m^{-1} . |
| a_p | absorption coefficient of particulate matter, m^{-1} . |
| $a_\varphi, \hat{a}_\varphi$ | measured and modeled, respectively, absorption coefficient of in vivo phytoplankton pigments, m^{-1} . |
| a_T, b_T, c_T | measured total light absorption, scattering and attenuation coefficients, respectively, excluding the influences of water, m^{-1} . |
| c_p | particulate attenuation coefficient, m^{-1} . |
| chl-a | chlorophyll a, mg m^{-3} . |
| λ | wavelength, nm. |
| $S_{\text{CDOM}}, S_{\text{CPM}}$ | spectral slope parameter for chromophoric dissolved and particulate matter absorption, respectively, nm^{-1} . |
| γ | hyperbolic spectral slope parameter for particulate attenuation spectra, dimensionless. |
| P | the matrix of hydrographic and optical properties of source water types. |
| y | solution vector returning fractional contributions of source water types to a mixture. |
| u | vector of hydrographic and optical properties of the mixture given y . |

[48] **Acknowledgments.** The authors wish to thank James Murray for the opportunity of participating on the Zonal Flux Cruise, the captain and

crew of the R/V Thompson for their assistance, and Zackary Johnson for use of his equipment. The authors thank François Baratange for technical assistance. This manuscript greatly benefited from critical and constructive comments of Heidi Sosik and Annick Bricaud. This work was funded by grants to CSR and WSP by the Environmental Optics Program of the Office of Naval Research.

References

- Allali, K., A. Bricaud, and H. Claustre, Spatial variations in the chlorophyll-specific absorption coefficients of phytoplankton and photosynthetically active pigments in the equatorial Pacific, *J. Geophys. Res.*, **102**, 12,413–12,423, 1997.
- Archer, D. E., E. T. Peltzer, and D. L. Kirchman, A timescale for dissolved organic carbon production in equatorial Pacific surface waters, *Global Biogeochem. Cycles*, **11**, 435–452, 1997.
- Babin, M., and D. Stramski, Light absorption by aquatic particles in the near-infrared spectral region, *Limnol. Oceanogr.*, **47**, 911–915, 2002.
- Babin, M., D. Stramski, G. M. Ferrari, H. Claustre, A. Bricaud, Obolensky, and N. Hoepffner, Variations in the light absorption coefficients of phytoplankton, nonalgal particles, and dissolved organic matter in coastal waters around Europe, *J. Geophys. Res.*, **108**(C7), 3211, doi:10.1029/2001JC000882, 2003.
- Boss, E., W. S. Pegau, W. D. Gardner, J. R. V. Zaneveld, A. H. Barnard, M. S. Twardowski, G. C. Chang, and T. D. Dickey, Spectral particulate attenuation and particle size distribution in the bottom boundary layer of a continental shelf, *J. Geophys. Res.*, **106**, 9509–9516, 2001.
- Bricaud, A., A. Morel, and L. Prieur, Absorption by dissolved organic matter of the sea (yellow substance) in the UV and visible domains, *Limnol. Oceanogr.*, **26**, 43–53, 1981.
- Bricaud, A., M. Babin, A. Morel, and H. Claustre, Variability in the chlorophyll-specific absorption coefficients of natural phytoplankton: Analysis and parameterization, *J. Geophys. Res.*, **100**, 13,321–13,332, 1995a.
- Bricaud, A., C. S. Roesler, and J. R. V. Zaneveld, In situ methods for measuring the inherent optical properties of ocean waters, *Limnol. Oceanogr.*, **40**, 393–410, 1995b.
- Bricaud, A., A. Morel, M. Babin, K. Allali, and H. Claustre, Variations of light absorption by suspended particles with the chlorophyll a concentration in oceanic (case I) waters: Analysis and implications for bio-optical models, *J. Geophys. Res.*, **103**, 31,033–31,044, 1998.
- Bricaud, A., C. S. Roesler, J. S. Parslow, and J. Ishizaka, Bio-optical studies during the JGOFS-equatorial Pacific program: A contribution to the knowledge of the equatorial system, *Deep Sea Res., Part II*, **49**, 2583–2599, 2002.
- Carder, K. L., R. G. Steward, G. R. Harvey, and P. B. Ortner, Marine humic and fulvic acids: Their effects on remote sensing of ocean chlorophyll, *Limnol. Oceanogr.*, **34**, 68–81, 1989.
- Carr, M., N. S. Oakey, B. Jones, and M. R. Lewis, Hydrographic patterns and vertical mixing in the equatorial Pacific along 150°W, *J. Geophys. Res.*, **97**, 611–626, 1992.
- Claustre, H., A. Morel, M. Babin, C. Cailliau, and D. Marie, Variability in particle attenuation and chlorophyll fluorescence in the tropical Pacific: Scales, patterns, and biogeochemical implications, *J. Geophys. Res.*, **104**, 3401–3422, 1999.
- Druffel, E. R., P. M. Williams, J. E. Bauer, and J. R. Ertel, Cycling of dissolved and particulate organic matter in the open ocean, *J. Phys. Oceanogr.*, **97**, 15,639–15,659, 1992.
- Dupouy, C., J. Neveux, and J. M. André, Spectral absorption coefficient of photosynthetically active pigments in the equatorial Pacific Ocean (165°E–150°W), *Deep Sea Res.*, **44**, 1881–1906, 1997.
- Dupouy, C., H. Loisel, J. Neveux, S. L. Brown, C. Moulin, J. Blanchot, A. Le Bouteiller, and M. R. Landry, Microbial absorption and backscattering coefficients from in situ and POLDER satellite data during an El Niño-Southern Oscillation cold phase in the equatorial Pacific (180°), *J. Geophys. Res.*, doi:10.1029/2001JC001298, in press, 2003.
- DuRand, M. D., and R. J. Olson, Contributions of phytoplankton light scattering and cell concentration changes to diel variations in beam attenuation in the equatorial Pacific from flow cytometric measurements of pico-, ultra-, and nanoplankton, *Deep Sea Res., Part II*, **43**, 891–906, 1996.
- Guo, L., P. H. Santschi, and K. W. Warnken, Dynamics of dissolved organic carbon (DOC) in oceanic environments, *Limnol. Oceanogr.*, **40**, 1392–1403, 1995.
- Guo, L., P. H. Santschi, L. A. Cifuentes, S. E. Trumbore, and J. Southon, Cycling of high-molecular-weight dissolved organic matter in the middle Atlantic Bight as revealed by carbon isotopic (¹³C and ¹⁴C) signatures, *Limnol. Oceanogr.*, **41**, 1242–1252, 1996.
- Harimoto, T., J. Ishizaka, and R. Tsuda, Latitudinal and vertical distributions of phytoplankton absorption spectra in the North Pacific during spring 1994, *J. Oceanogr.*, **55**, 667–679, 1999.
- Hoge, F. E., A. V. Vodacek, and N. Blough, Inherent optical properties of the ocean: Retrieval of the absorption coefficient of chromophoric dissolved organic matter from fluorescence measurements, *Limnol. Oceanogr.*, **38**, 1394–1402, 1993.
- Holm-Hansen, O., C. J. Lorenzen, R. W. Holmes, and J. D. Strickland, Fluorometric determination of chlorophyll, *J. Cons. Int. Explor. Mer.*, **30**, 3–15, 1965.
- Honjo, S., S. J. Manganini, and L. J. Poppe, Sedimentation of lithogenic particles in the open sea, *Mar. Geol.*, **50**, 199–220, 1982.
- Kishino, M., M. Takahashi, N. Okami, and S. Ichimura, Estimation of the spectral absorption coefficients of phytoplankton in the sea, *Bull. Mar. Sci.*, **37**, 634–642, 1985.
- Kitchen, J. C., and J. R. V. Zaneveld, On the non-correlation of the vertical structure of light scattering and chlorophyll a in case I waters, *J. Geophys. Res.*, **95**, 20,237–20,246, 1990.
- Landry, M. R., et al., Iron and grazing constraints on primary production in the central equatorial Pacific: An EqPac synthesis, *Limnol. Oceanogr.*, **42**, 405–419, 1997.
- Lorenzen, C. J., and J. N. Downs, The specific absorption coefficients of chlorophyllide a and pheophorbide a in 90% acetone, and comments on the fluorometric determination of chlorophyll and pheopigments, *Limnol. Oceanogr.*, **31**, 449–452, 1986.
- Mackas, D. L., K. L. Denman, and A. F. Bennett, Least squares multiple tracer analysis of water mass composition, *J. Geophys. Res.*, **92**, 2907–2918, 1987.
- Miller, W., and M. Moran, Interaction of photochemical and microbial processes in the degradation of refractory dissolved organic matter from a coastal marine environment, *Limnol. Oceanogr.*, **42**, 1317–1324, 1997.
- Montgomery, M. T., N. A. Welschmeyer, and D. L. Kirchman, A simple assay for chitin: Application to sediment trap samples from the subarctic Pacific, *Mar. Ecol. Prog. Ser.*, **64**, 301–308, 1990.
- Mopper, K., and C. Schultz, Fluorescence as a possible tool for studying the nature and water column distribution of DOC components, *Mar. Chem.*, **41**, 229–238, 1993.
- Mopper, K., X. Zhou, R. Kieber, R. Sikorski, and R. Jones, Photochemical degradation of organic carbon and its impact on the oceanic carbon cycle, *Nature*, **353**, 60–62, 1991.
- Mopper, K., J. Zhou, J. S. Ramana, U. Passow, H. G. Dam, and D. T. Drapeau, The role of surface-active carbohydrates in the flocculation of a diatom bloom in a mesocosm, *Deep Sea Res.*, **42**, 47–73, 1995.
- Morel, A., and L. Prieur, Analysis of variations in ocean colour, *Limnol. Oceanogr.*, **22**, 709–722, 1977.
- Murray, J. W., R. T. Barber, M. R. Roman, M. P. Bacon, and R. A. Feely, Physical and biological controls on carbon cycling in the equatorial Pacific, *Science*, **266**, 58–65, 1994.
- Nelson, N., and D. Siegel, Chromophoric DOM in the open ocean, *Biogeochemistry of Marine Dissolved Organic Matter*, edited by D. A. Hansell and C. A. Carlson, pp. 547–573, Academic, San Diego, Calif., 2002.
- Parslow, J. S., L. A. Clementson, A. R. Turnbull, and D. C. McKenzie, Bio-optical characteristics of oceans around Australia, paper presented at the Ocean Optics XIV Conference, Hawaii, 1998.
- Pegau, W. S., The distribution of colored dissolved organic matter (CDOM) in the equatorial Pacific, *Proc. SPIE-Int. Soc. Opt. Eng.*, **2963**, 508–513, 1997.
- Pegau, W. S., and J. R. V. Zaneveld, Temperature-dependent absorption of water in the red and near-infrared portions of the spectrum, *Limnol. Oceanogr.*, **38**, 188–192, 1993.
- Pegau, W. S., et al., A comparison of methods for the measurement of the absorption coefficient in natural waters, *J. Geophys. Res.*, **100**, 13,201–13,220, 1995.
- Pegau, W. S., D. Gray, and J. R. V. Zaneveld, Absorption and attenuation of visible and near-infrared light in water: Dependence on temperature and salinity, *Appl. Opt.*, **36**, 6035–6046, 1997.
- Reverdin, G., C. Frankignoul, E. Kestenare, and M. J. McPhaden, Seasonal variability in the surface currents of the equatorial Pacific, *J. Geophys. Res.*, **99**, 20,323–20,344, 1994.
- Roesler, C. S., Theoretical and experimental approaches to improve the accuracy of particulate absorption coefficients derived from the quantitative filter technique, *Limnol. Oceanogr.*, **43**, 1649–1660, 1998.
- Roesler, C. S., and M. J. Perry, In situ phytoplankton absorption, fluorescence emission, and particulate backscattering spectra determined from reflectance, *J. Geophys. Res.*, **100**, 13,279–13,294, 1995.
- Roesler, C. S., M. J. Perry, and K. L. Carder, Modeling in situ phytoplankton absorption from total absorption spectra in productive inland marine waters, *Limnol. Oceanogr.*, **34**, 1510–1523, 1989.
- Roesler, C. S., J. Simeon, and M. C. Talbot, Variability in vertical distributions of size fractionated component absorption and scattering coefficients in shallow continental shelf waters, paper presented at the ASLO Aquatic

- Sciences Meeting, Am. Soc. of Limnol. And Oceanogr., Santa Fe, N. M., 1997.
- Siegel, D. A., T. D. Dickey, L. Washburn, M. K. Hamilton, and B. G. Mitchell, Optical determination of particulate abundance and production variations in the oligotrophic ocean, *Deep Sea Res.*, *36*, 211–222, 1989.
- Siegel, D. A., S. Maritorena, N. Nelson, D. A. Hansell, and M. Lorenzi-Kayser, Global distribution and dynamics of colored dissolved and detrital organic materials, *J. Geophys. Res.*, *107*, 3228–3241, 2002.
- Simeon, J., Decomposition of absorption coefficients and decorrelation lengthscales of hydrographic and inherent optical properties in the middle Atlantic Bight, M. S. thesis, Oregon State Univ., Corvallis, Ore., 2001.
- Skoog, A., and R. Benner, Aldoses in various size fractions of marine organic matter: Implications for carbon cycling, *Limnol. Oceanogr.*, *42*, 1803–1813, 1997.
- Sosik, H. M., R. E. Green, W. S. Pegau, and C. S. Roesler, Temporal and vertical variability in optical properties of New England shelf waters during late summer and spring, *J. Geophys. Res.*, *106*, 9455–9472, 2001.
- Stramski, D., and R. Reynolds, Diel variations in the optical properties of a marine diatom, *Limnol. Oceanogr.*, *38*, 1347–1364, 1993.
- Stramski, D., F. Rasoulzadegan, and D. A. Kiefer, Changes in the optical properties of a particle suspension caused by protist grazing, *J. Plankton Res.*, *14*, 961–977, 1992.
- Stramski, D., A. Shalapyonok, and R. A. Reynolds, Optical characterization of the oceanic unicellular cyanobacterium *Synechococcus* grown under a day-night cycle in natural irradiance, *J. Geophys. Res.*, *100*, 13,295–13,307, 1995.
- Stramski, D., A. Bricaud, and A. Morel, Modeling the inherent optical properties of the ocean based on the detailed composition of planktonic community, *Appl. Opt.*, *40*, 2929–2945, 2001.
- Thompson, R. O. R. Y., and R. J. Edwards, Mixing and water mass formation in the Australian Subantarctic, *J. Phys. Oceanogr.*, *11*, 1399–1406, 1981.
- Welschmeyer, N. A., Fluorometric analysis of chlorophyll a in the presence of chlorophyll b and phaeopigments, *Limnol. Oceanogr.*, *38*, 1985–1992, 1994.
- Williams, P. M., and E. R. Druffel, Radiocarbon in dissolved organic matter in the central North Pacific Ocean, *Nature*, *330*, 246–248, 1987.
- Wyrski, K., and B. Kilonsky, Mean water and current structure during the Hawaii to Tahiti shuttle experiment, *J. Phys. Oceanogr.*, *14*, 242–254, 1984.
-
- C. Dupouy, Centre IRD de Noumea, BP A5 Noumea, New Caledonia. (cecile.dupouy@noumea.ird.nc)
- W. S. Pegau, Kachemak Bay Research Reserve, 2181 Kachemak Dr., Homer, AK 99603, USA. (spegau@oce.orst.edu)
- C. Roesler, Bigelow Laboratory for Ocean Sciences, P.O. Box 475, West Boothbay Harbor, ME 04575, USA. (croesler@bigelow.org)
- J. Simeon, Atmospheric and Oceanic Sciences Program, Princeton University, P.O. Box CN 710, Princeton, NJ 08544, USA. (jsimeon@princeton.edu)